Effect of adsorbates on surface phonon modes: H on Pd(001) and Pd(110)

W. Zhong, Y. S. Li,* and D. Tománek
Department of Physics and Astronomy, Michigan State University, East Lansing, Michigan 48824-1116
and Center for Fundamental Materials Research, Michigan State University, East Lansing, Michigan 48824-1116
(Received 3 July 1991)

We investigate the effect of adsorbates on surface vibrations by calculating the phonon spectra of clean and hydrogen-covered (001) and (110) surfaces of Pd. The dynamical matrix of these systems is determined using a model many-body alloy Hamiltonian based on *ab initio* density-functional results for these systems, with no adjustable parameters for surface properties. The most pronounced effect of hydrogen is a strong softening of the Rayleigh wave on Pd(001) and a hardening of surface modes on Pd(001) and Pd(110) with vibration amplitudes confined to the surface layer.

I. INTRODUCTION

The interaction of hydrogen with transition metals is a fundamentally interesting topic with wide ranging technological applications.[1] The particular interest in Pd is motivated to a large degree by the ability of this metal to form hydrides and thereby to act as a medium for hydrogen storage. Hydrogen embrittlement, on the other hand, is a matter of great concern.[2] The crucial step in the process of bulk hydride formation, which has received most attention, involves the dissociative adsorption of hydrogen on the surface.

Extensive studies of the adsorbate phase include the characterization of the H-metal bond, hydrogen-induced surface relaxation and reconstruction, and effect of hydrogen on the electronic structure of the metal substrate.[3–13] So far, most research effort has been focused on the adsorption geometry and on the electronic and structural properties. Surface phonons have received far less attention in the recent literature, in spite of the wealth of information they contain about the nature of bonding at surfaces. This is caused mainly by the difficulty to measure and calculate reliable surface phonon dispersion curves throughout the whole surface Brillouin zone.

Only recently, He time-of-flight spectroscopy[14–17] and electron-energy-loss spectroscopy[18–21] (EELS) have been used to measure the dispersion curves of surface phonons on a variety of metal substrates. The quantitative interpretation of these data is lacking in most cases, since predictive *ab initio* calculations (such as "frozen-phonon" calculations) are computationally very involved. Only in selected cases, local-density approximation[22] (LDA) calculations have been performed for the high-symmetry modes.[23]

The majority of published phonon calculations use lattice dynamics based on simple two- and three-body potentials.[24–27] These types of calculations use bulk and surface interatomic force constants and distances as independent parameters which are chosen to fit the experimental results.[15] In general, these calculations show good agreement with the observed data. The predictive power is limited by the generally large number of force-constant parameters that depend on the model, the system, and the surface studied. While these calculations can provide a rough guidance in the interpretation of experimental results, direct comparisons between different models are of limited use.

More recently, the embedded-atom method[28] (EAM) has been used to calculate phonon dispersion relations on surfaces such as Cu(100), Cu(111), and Ag(111).[29–31] The major difference to the calculations quoted above is that all parameters have been obtained by fitting the measured bulk properties. The EAM has proven to be quite successful in the prediction of surface phonon spectra and the corresponding changes of interatomic force constants and distances at surfaces. The major weakness of these calculations is the limitation to single-component systems, since charge transfers between different sites are assumed to be zero. Of less importance is the fact that the success of the EAM technique depends on the type of experimental data and the fit used to reproduce bulk properties.

In this paper, we develop a model many-body alloy (MBA) Hamiltonian, based on *ab initio* calculations of bulk materials (both single component and alloys). This Hamiltonian is used to determine the structural relaxations and phonon spectra of clean and hydrogen covered surfaces of Pd. We show that the MBA Hamiltonian can be easily applied to many alloy systems, and can be uniquely determined from a set of *ab initio* calculations with no free parameters.

This paper is structured as follows. In Sec. II, we derive the many-body alloy Hamiltonian and summarize the procedure to calculate surface phonons. In Sec. III, we determine the parameters in the MBA Hamiltonian using *ab initio* results for the equilibrium structure and binding energy of bulk materials, with specific emphasis on the H/Pd system. We test this Hamiltonian by calculating the equilibrium structure and energy of bulk Pd and PdH, as well as H-free and H-covered Pd(001) and Pd(110) surfaces. In Sec. IV, we calculate the phonon

spectra for bulk Pd and PdH, as well as the clean and H-covered Pd(001) and Pd(110) surfaces. Finally, in Sec. V, we conclude this paper with general remarks.

II. THE MANY-BODY ALLOY HAMILTONIAN

The many-body alloy Hamiltonian is an extension of a total energy scheme, which has been successfully used previously to study the electronic and structural properties of small clusters, surfaces of metals, and dilute metal alloys.[32–35] As discussed earlier,[32–34] the total cohesive energy of the crystal can be decomposed into individual atomic binding energies $E_{\rm coh}(i)$, as

$$E_{\rm coh}({\rm tot}) = \sum_i E_{\rm coh}(i). \tag{1}$$

The binding energy of atom i consists of an attractive part due to the hybridization of orbitals, $E^{BS}(i)$, and a term $E^R(i)$ describing repulsive interactions. We have

$$E_{\rm coh}(i) = E^{BS}(i) + E^R(i). \tag{2}$$

Different simplified parametrization forms have been proposed[36] for the many-body energy $E^{BS}(i)$. The embedded-atom scheme[28] takes $E^{BS}(i)$ as a unique function of the total charge density of the unperturbed host at the site i. Since this parametrization might cause problems in the case of alloys with nonzero charge transfer, we base our expression for $E^{BS}(i)$ on a tight-binding Hamiltonian. In a one-electron picture, the binding energy of atom i is given by an integral over the local density of states at i, $N_i(E)$, as

$$E^{BS}(i) = -\int_{-\infty}^{E_F} (E - E_0) N_i(E) dE. \tag{3}$$

In the second-moment approximation, $E^{BS}(i)$ is proportional to the effective bandwidth, which in turn is proportional to the square root of the second moment $M_2(i)$ of the local density of states. We obtain

$$E^{BS}(i) \propto M_2(i)^{1/2} = \left(\sum_{j\neq i} t_{ij}^2\right)^{1/2} \propto \left(\sum_{j\neq i} e^{-2qr_{ij}}\right)^{1/2}. \tag{4}$$

In the last part of this equation, we have related M_2 to the hopping integral t_{ij} between neighboring sites i and j and assumed an exponential distance dependence of the effective (screened) hopping integrals, as $t(r) \propto e^{-qr}$.

The repulsive part is parametrized by a pairwise Born-Mayer potential with an exponential distance dependence, as

$$E^R(i) \propto \sum_{j\neq i} e^{-pr_{ij}}. \tag{5}$$

We obtain

$$\begin{aligned} E_{\rm coh}(i) &= E^{BS}(i) + E^R(i) \\ &= -\left\{\sum_{j\neq i} \xi_0^2 \exp\left[-2q\left(\frac{r_{ij}}{r_0} - 1\right)\right]\right\}^{1/2} \\ &\quad + \varepsilon_0^R \sum_{j\neq i} \exp\left[-p\left(\frac{r_{ij}}{r_0} - 1\right)\right]. \end{aligned} \tag{6}$$

Here, r_{ij} is the distance between atoms i and j. Parameters p and q describe the distance dependence of the hopping integrals and the Born-Mayer interactions, respectively, and are related to the bulk elastic properties. In the case of a single-component bulk crystal, Eq. (6) can be used to reproduce the equilibrium properties, such as the equilibrium nearest-neighbor distance r_0 and the bulk cohesive energy $E_{\rm coh}({\rm bulk})$. In this case, assuming isotropic hopping integrals, ξ_0 and ε_0^R in Eq. (6) are given by

$$\xi_0 = \frac{E_{\rm coh}({\rm bulk})}{(1 - q/p)(Z_{\rm bulk})^{1/2}}, \tag{7}$$

$$\varepsilon_0^R = \frac{\xi_0}{Z_{\rm bulk}^{1/2}} \frac{q}{p}, \tag{8}$$

where $Z_{\rm bulk}$ is the bulk coordination number.

For systems with more than one component (such as alloys and compounds), Eq. (6) can be generalized to

$$\begin{aligned} E_{\rm coh}(i,\alpha) = &-\left\{\sum_{j\neq i} \xi_{0,\alpha\beta}^2 \exp\left[-2q_{\alpha\beta}\left(\frac{r_{ij,\alpha\beta}}{r_{0,\alpha\beta}} - 1\right)\right]\right\}^{1/2} \\ &+ \sum_{j\neq i} \varepsilon_{0,\alpha\beta}^R \exp\left[-p_{\alpha\beta}\left(\frac{r_{ij,\alpha\beta}}{r_{0,\alpha\beta}} - 1\right)\right], \end{aligned} \tag{9}$$

where α and β represent the types of atoms i and j, respectively.

As we discussed above, the Hamiltonian underlying the energy expression in Eq. (9) describes the essential physics governing cohesion in many solids. The large flexibility and the microscopic basis for the description of many-body attractive interactions in alloys makes the MBA Hamiltonian superior to embedded-atom-like schemes[28,36] for two main reasons. First, unlike the EAM,[28] Eq. (9) does distinguish the binding changes of atom i surrounded either by Z_α atoms of type α or Z_β atoms of type β even in the case that the charge density at site i due to the surrounding atoms is the same. Second, in contrast to the EAM, our approach does not assume local charge neutrality in alloys. For this reason, we feel confident to apply this energy expression as a physically sensible interpolation scheme to determine the energy of structures with low symmetry, once the corresponding *ab initio* data for high symmetry structures are available. Specifically, we will use this energy expression to find total energy changes due to small lattice distortions in the case of a phonon calculation for the Pd-H system which we describe below.

The phonon spectrum can be obtained from the dynamical matrix.[37] The dynamical matrix $D(\mathbf{k})$, corresponding to wave vector $\mathbf{k}$, is given by

$$\begin{aligned} D_{\alpha\beta,\kappa\nu}(\mathbf{k}) = &(M_\kappa M_\nu)^{-1/2} \\ &\times \sum_{\mathbf{R}_i - \mathbf{R}_j} \Phi_{\alpha\beta,i\kappa,j\nu} \exp[-i\mathbf{k}\cdot(\mathbf{R}_i - \mathbf{R}_j)]. \end{aligned} \tag{10}$$

Here, M_κ is the mass of the κth atom and M_ν is the mass of the νth atom. $\Phi_{\alpha\beta,i\kappa,j\nu}$ is the force-constant matrix, which can be expressed as

$$\Phi_{\alpha\beta,i\kappa,j\nu} = \frac{\partial^2 E_{\rm coh}({\rm tot})}{\partial u_{\alpha,i\kappa}\partial u_{\beta,j\nu}}, \tag{11}$$

where $E_{\rm coh}$(tot) is the total energy of the system. $u_{\alpha,i\kappa}$ is the αth Cartesian component of the displacement of the κth atom in the ith unit cell, and $u_{\beta,j\nu}$ is the βth Cartesian component of the displacement of the νth atom in the jth unit cell.

Finally, the phonon frequencies $\omega(\mathbf{k})$ are related to the eigenvalues of $D(\mathbf{k})$, given by

$$\det|\omega^2(\mathbf{k})\underline{I} - \underline{D}(\mathbf{k})| = 0. \tag{12}$$

III. APPLICATION OF THE MANY-BODY ALLOY HAMILTONIAN TO THE Pd-H SYSTEM

In this section, we first determine the parameters of the MBA Hamiltonian for the Pd-H system, based on our *ab initio* results[3–5] for the structure and cohesive energy of bulk Pd and PdH. It should be noted that this procedure does not allow free parameters. We apply this Hamiltonian next to determine structural and bonding properties of clean and hydrogen-covered Pd surfaces.

A. Construction of the MBA Hamiltonian

In the MBA Hamiltonian, each of the H-H, H-Pd, and Pd-Pd interactions is characterized by a set of five parameters: ξ_0, ε_0^R, q, p, and r_0 (four of these parameters are independent). The Pd-Pd interaction is obtained from our previous *ab initio* calculation[5] of the cohesive energy $E_{\rm coh}$ as a function of the lattice constant a for bulk Pd. We consider nearest-neighbor interactions only and obtain a simplified expression for the bulk cohesive energy, $E_{\rm coh}$(Pd bulk)

$$\begin{aligned} &= -\left\{ Z_{\rm bulk}\,\xi^2_{0,\text{Pd-Pd}} \right. \\ &\qquad \left. \times \exp\left[-2q_{\rm Pd,Pd}\left(\frac{r_{\text{Pd-Pd}}}{r_{0,\text{Pd-Pd}}} - 1\right)\right]\right\}^{1/2} \\ &\quad + Z_{\rm bulk}\,\varepsilon^R_{0,\text{Pd-Pd}} \exp\left[-p\left(\frac{r_{\text{Pd-Pd}}}{r_{0,\text{Pd-Pd}}} - 1\right)\right] . \end{aligned} \tag{13}$$

Here, $Z_{\rm bulk} = 12$ for the fcc structure and $r_{0,\text{Pd-Pd}} = a\sqrt{2}/2$ is the nearest-neighbor distance. The calculated cohesive energy $E_{\rm coh}$ of bulk Pd as a function of the lattice constant a is given by the solid line in Fig. 1 and compared to corresponding LDA results of Ref. 5. The parameters used in Eq. (13) are given in Table I.

The parameters for H-H interaction can be determined in a similar way, by mapping the MBA Hamiltonian to the *ab initio* calculation of hydrogen on a lattice. The corresponding parameters are given in Table I.

To determine the parameters for the Pd-H interaction, we apply the MBA Hamiltonian to bulk PdH. Considering the nearest-neighbor Pd-H, H-H, and Pd-Pd interactions, we can obtain the cohesive energy of the PdH crystal with NaCl structure as

$$E_{\rm coh} = E_{\rm coh}({\rm H}) + E_{\rm coh}({\rm Pd}). \tag{14}$$

The binding energies of H and Pd in this structure are given by

$$\begin{aligned} E_{\rm coh}({\rm H}) = &-\left\{ Z_{\rm H}({\rm Pd})\xi^2_{0,\text{Pd-H}} \exp\left[-2q_{\rm Pd,H}\left(\frac{r_{\text{Pd-H}}}{r_{0,\text{Pd-H}}} - 1\right)\right] + Z_{\rm H}({\rm H})\xi^2_{0,\text{H-H}} \exp\left[-2q_{\rm H,H}\left(\frac{r_{\text{H-H}}}{r_{0,\text{H-H}}} - 1\right)\right]\right\}^{1/2} \\ &+\left\{ Z_{\rm H}({\rm Pd})\varepsilon^R_{0,\text{Pd-H}} \exp\left[-p_{\rm Pd,H}\left(\frac{r_{\text{Pd-H}}}{r_{0,\text{Pd-H}}} - 1\right)\right] + Z_{\rm H}({\rm H})\varepsilon^R_{0,\text{H-H}} \exp\left[-p_{\rm H,H}\left(\frac{r_{\rm HH}}{r_{0,\text{H-H}}} - 1\right)\right]\right\} \end{aligned} \tag{15}$$

and

$$\begin{aligned} E_{\rm coh}({\rm Pd}) = &-\left\{ Z_{\rm Pd}({\rm H})\xi^2_{0,\text{Pd-H}} \exp\left[-2q_{\rm Pd,H}\left(\frac{r_{\text{Pd-H}}}{r_{0,\text{Pd-H}}} - 1\right)\right] + Z_{\rm Pd}({\rm Pd})\xi^2_{0,\text{Pd-Pd}} \exp\left[-2q_{\rm Pd,Pd}\left(\frac{r_{\text{Pd-Pd}}}{r_{0,\text{Pd-Pd}}} - 1\right)\right]\right\}^{1/2} \\ &+\left\{ Z_{\rm Pd}({\rm H})\varepsilon^R_{0,\text{Pd-H}} \exp\left[-p_{\rm Pd,H}\left(\frac{r_{\text{Pd-H}}}{r_{0,\text{Pd-H}}} - 1\right)\right] + Z_{\rm Pd}({\rm Pd})\varepsilon^R_{0,\text{Pd-Pd}} \exp\left[-p_{\rm Pd,Pd}\left(\frac{r_{\text{Pd-Pd}}}{r_{0,\text{Pd-Pd}}} - 1\right)\right]\right\} . \end{aligned} \tag{16}$$

TABLE I. Interaction parameters used in the many-body alloy Hamiltonian for the Pd-H system.

Interaction	$q_{\alpha\beta}$	$p_{\alpha\beta}$	$r_{\alpha\beta,0}$ (Å)	$\varepsilon^R_{\alpha\beta}$ (eV)	$\xi_{\alpha\beta}$ (eV)
Pd-Pd	3.40	14.8	2.758	0.08376	1.2630
H-H	3.22	5.28	2.300	0.1601	0.9093
H-Pd	2.20	5.50	1.769	0.6794	2.5831

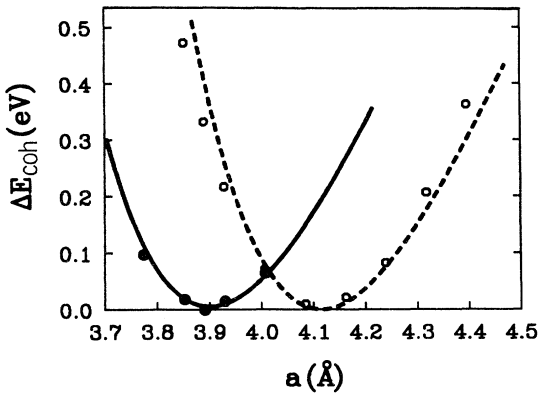

FIG. 1. Cohesive energy changes $\Delta E_{\rm coh} = E_{\rm coh} - E_{\rm coh,0}$ in bulk Pd and PdH as a function of the lattice constant a. Values obtained using the MBA Hamiltonian for Pd (solid line) and PdH (dashed line) are compared to LDA results of Ref. 5 for the corresponding systems, given by • and o.

Here, $Z_{\rm Pd}({\rm H}) = 6$ and $Z_{\rm Pd}({\rm Pd}) = 12$ are the respective numbers of H and Pd nearest neighbors of a Pd atom, and $Z_{\rm H}({\rm Pd}) = 6$ and $Z_{\rm H}({\rm H}) = 12$ are the numbers of H and Pd nearest neighbors of a H atom. $r_{0,\text{Pd-H}} = a/2$ and $r_{0,\text{Pd-Pd}} = a\sqrt{2}/2$ are the Pd-H and Pd-Pd nearest-neighbor distances and a is the lattice constant. The values of $\xi_{0,\text{Pd-H}}$, $p_{\rm Pd,H}$, $q_{\rm Pd,H}$, and $\varepsilon^R_{0,\text{Pd-H}}$ have been determined by reproducing LDA results of Ref. 5 for $E_{\rm coh}$ of bulk PdH and are given in Table I. The corresponding results obtained with the MBA Hamiltonian are given by the dashed line in Fig. 1, together with the LDA results given by the data points. The good agreement between results for the bulk systems based on the MBA method and LDA calculations indicates that the model Hamiltonian has sufficient flexibility to describe energy changes accurately.

B. Structural and energetic properties of clean and H-covered Pd(001) and Pd(110) surfaces

In the preceding section, we have constructed the MBA Hamiltonian and shown that it can reproduce the bulk equilibrium properties very accurately. In this section, we test its applicability to surfaces, specifically to the calculation of surface energies, surface relaxations, and adsorption energies on (001) and (110) surfaces of Pd. Our results will be compared to experimental data and to *ab initio* data of Refs. 3 and 5.

The surface energy of a clean Pd surface is related to the cohesive energy of the bulk and of an n-layer slab by[5]

$$E_s = \tfrac{1}{2}[E_{\rm coh}(\text{Pd slab}) - nE_{\rm coh}(\text{Pd bulk})]. \qquad (17)$$

We have assumed that the slab energy $E_{\rm coh}$(Pd slab) and the corresponding surface energy E_s are *per surface atom*. Using this equation together with Eqs. (1) and (6), we can easily determine the surface energy for a given Pd surface, and also the multilayer surface relaxations by minimizing E_s.

Here, we have calculated the surface energy for Pd slabs with both (001) and (110) surfaces. Our results for the change of the surface energy ΔE_s corresponding to a relaxation Δd_{12} of the topmost Pd interlayer distance are given in Fig. 2. The calculations for the (001) and (110) surfaces of Pd are given by the solid lines in Figs. 2(c) and 2(d), respectively. For the sake of simple comparison with the LDA results of Ref. 5 [given by the data points in Fig. 2(d)], these model calculations have been performed for a three-layer Pd slab. Our results indicate a surface contraction which increases with a decreasing coordination number of the surface atoms, in quantitative agreement with the LDA data.

In principle, we can easily handle very thick slabs with the MBA Hamiltonian and will concentrate on much thicker slabs with $n = 25$ in our calculation. This slab thickness is more than sufficient to guarantee that the two slab surfaces do not interact and that the atoms in the middle of the slab are in a truly bulk environment.

Our numerical results indicate that the surface energy of Pd(110) (0.73 eV/atom) is much higher than that of Pd(001) (0.48 eV/atom). As discussed in more detail in Ref. 5, this can be tracked back to the narrowing of the effective Pd $4d$ band width or an increasing number of "dangling bonds" with decreasing coordination number. Since precise experimental data for these surface energies are not available, we will only compare our results with recent LDA calculations.[5] For Pd(001), our surface energy value $E_s = 0.48$ eV/atom is very close to the LDA

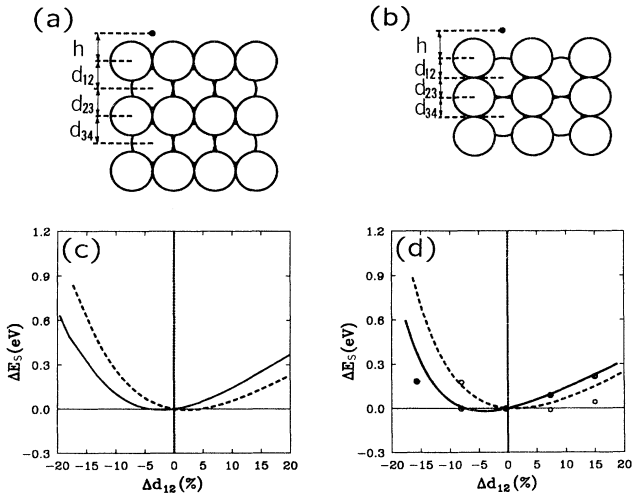

FIG. 2. Schematic side view of the (a) Pd(001) and (b) Pd(110) surfaces showing the definitions of the hydrogen adsorption height h and the interlayer spacings d_{12}, d_{23}, and d_{34}. Surface energy changes $\Delta E_s = E_s - E_{s,0}$ for clean and H-covered (c) Pd(001) and (d) Pd(110) surfaces, as a function of the first interlayer spacing d_{12}. Values obtained using the MBA Hamiltonian for clean (solid line) and H-covered (dashed line) surfaces are compared to the LDA results of Ref. 5 for the corresponding systems, given by • and o.

TABLE II. Relaxations at clean and hydrogen covered Pd surfaces.

Surface	Δd_{12} (%)	Δd_{23} (%)	Δd_{34} (%)	Reference
Pd(001)	−2.2	0.2	0.0	Present work
Pd(110)	−5.2	0.7	−0.3	Present work
Pd(001) + $p(1\times1)$H	4.0	0.7	0.0	Present work
Pd(110) + $p(1\times1)$H	1.3	1.3	0.0	Present work
Pd(110)	−6.0±2	1.0±2		Ref. 39
Pd(110)	−5.1±1.5	2.9±1.5		Ref. 40
Pd(110) + (2×1)H	−2.2±1.5	2.9±1.5		Ref. 40

result[5] of 0.49 eV/atom. Our value E_s = 0.73 eV/atom for a Pd(110) surface is significantly lower than the reported LDA result of 1.80 eV/atom. The large discrepancy between these latter results is possibly due to a less adequate basis set and the neglect of surface relaxations in the LDA calculation.

The values in columns 2–4 of Table II indicate a damped oscillatory behavior for the surface relaxations. These oscillations occur as a general phenomenon which has been observed[38–40] and calculated[33,41] in many systems. We also find the surface relaxations to be more pronounced on the more open (110) surface than on the close-packed (001) surface, in agreement with the general observation that increasing relaxations correspond to larger surface energies. As seen in Table II, our calculated surface relaxations are in gratifying agreement with both experimental data[39,40] and LDA results.[5,41] This good agreement confirms that the MBA Hamiltonian can accurately describe the structure and energy changes of clean Pd(001) and Pd(110) surfaces.

Finally, we use the MBA Hamiltonian to determine the binding energy of hydrogen in different adsorption sites on the Pd(001) and Pd(110) surfaces. These calculations yield the preferential adsorption site and adsorption height, both of which are accessible to experimental verification. In order to simplify the comparison with the LDA calculations of Refs. 3 and 5, we performed all calculations for a three-layer Pd slab which is covered by H on both sides. We find the adsorption energy of H on Pd to be typically of the order $E_{ad} \approx -3$ eV. Since the binding energy of a H_2 molecule is only D_e = 4.75 eV, the dissociation probability of a H_2 molecule approaching the Pd surface is high. For this reason, we limit our investigations to atomic hydrogen on Pd(001) and Pd(110).

The equilibrium structure of hydrogen-covered surfaces can be determined in the same spirit as the calculation for the clean surfaces described above. Our results for the surface energies and multilayer relaxations are summarized in Fig. 2 and Table II. The hydrogen atoms are assumed to occupy the equilibrium sites during the surface relaxation. The calculated changes of the surface energy of hydrogen covered Pd(001) and Pd(110) surfaces are given by the dashed lines in Figs. 2(c) and 2(d), respectively. For the sake of simple comparison with the LDA results of Ref. 5 [given by the data points in Fig. 2(d)], these model calculations have been performed for a three-layer Pd slab. Our results indicate an expansion of the hydrogen-covered surfaces, in agreement with the LDA data. The reversal of surface contraction obtained for clean surfaces can be explained by the saturation of Pd dangling bonds by H atoms.

In Fig. 3, we display the adsorption energy of H on Pd(001) as a function of the adsorption height h for the on-top site, the bridge site, and the hollow site. Results

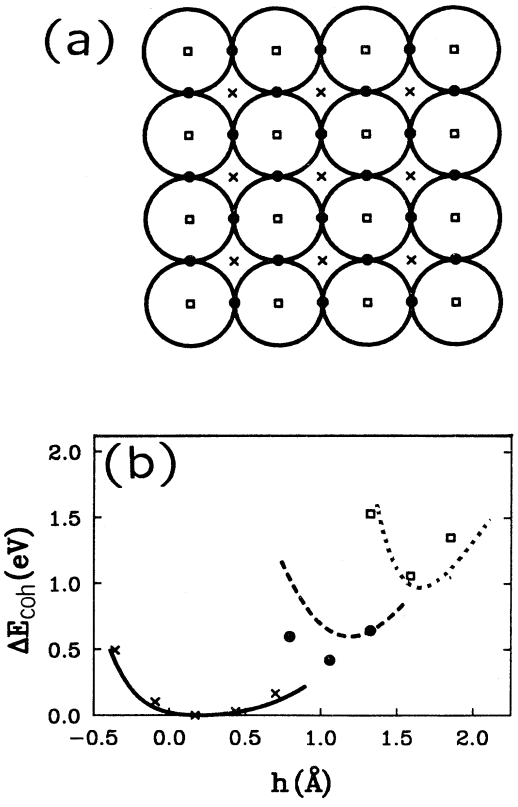

FIG. 3. (a) Schematic top view of the Pd(001) surface and the assignment of adsorption sites: hollow (×), bridge (•), and on-top (□). (b) Adsorption energy changes $\Delta E_{ad} = E_{ad} - E_{ad,0}$ (with respect to the equilibrium adsorption energy) as a function of the hydrogen adsorption height h on Pd(001). Results based on the MBA Hamiltonian for the hollow site (solid line), the bridge site (dashed line), and the on-top site (dotted line) are compared to LDA results of Refs. 3 and 5, given by the data points.

obtained using the MBA Hamiltonian, shown by lines, are compared to LDA data of Ref. 3, given by the data points. As discussed above, we represent the substrate by the same three-layer Pd slab as used in the LDA calculation. Since it is only energy differences which are relevant for the preferential adsorption sites and the vibration frequencies, we show adsorption energy changes $\Delta E_{ad} = E_{ad} - E_{ad,0}$ with respect to the adsorption energy of H in the equilibrium site in Fig. 3(b). We find the fourfold hollow site to be the equilibrium site on Pd(001), in agreement with the experimental data of Ref. 8 and the LDA results of Ref. 3. Also the very small equilibrium adsorption height $h_0 = 0.18$ Å above the first Pd layer is in good agreement with the LDA value[3] of 0.24 Å and the experimental result[13] of 0.30 Å. These small adsorption heights result from the very small atomic radius of hydrogen. More important, the MBA Hamiltonian gives H-Pd interaction potentials (and consequently vibration frequencies) in close agreement with the LDA data.

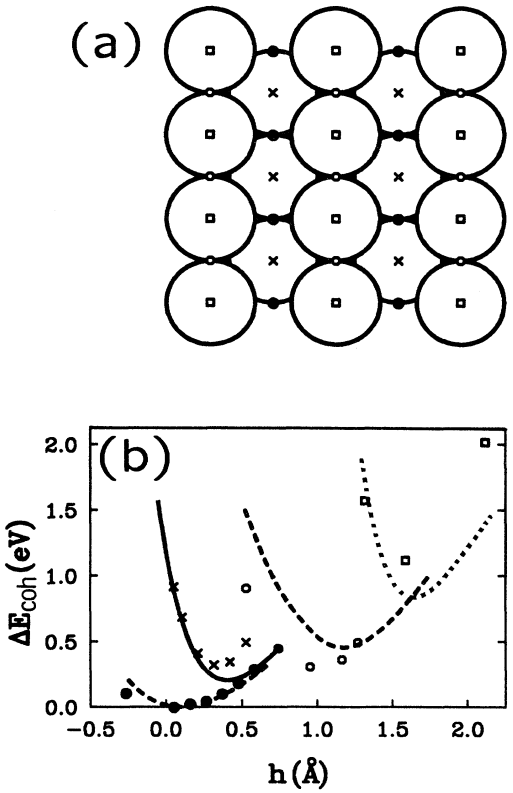

FIG. 4. (a) Schematic top view of the Pd(110) surface and the assignment of adsorption sites: hollow (×), long-bridge (•), short-bridge (o), and on-top (□). (b) Adsorption energy changes $\Delta E_{ad} = E_{ad} - E_{ad,0}$ (with respect to the equilibrium adsorption energy) as a function of the hydrogen adsorption height h on Pd(110). Results based on the MBA Hamiltonian for the hollow site (solid line), the long-bridge and the short-bridge sites (dashed line), and the on-top site (dotted line) are compared to LDA results of Ref. 5, given by the data points.

Adsorption energies for H on Pd(110) are shown in Fig. 4 for the on-top, the short-bridge, the long-bridge, and the hollow site. In analogy to Fig. 3, the continuous lines represent the MBA Hamiltonian results, and the discrete data points show LDA values of Ref. 5. Also in this case, the LDA and MBA Hamiltonian calculations have been performed for a three-layer Pd slab. Similar to the results for the (001) surface, the MBA potentials represent energy differences and adsorption potentials, which are in remarkably good agreement with the LDA data.

Both the MBA technique and LDA predict the long-bridge site to be the most favored among the adsorption sites considered here. Our calculation indicates that in this site, the equilibrium hydrogen adsorption height is only $h_0 = 0.09$ Å above the topmost Pd layer. Recent low-energy electron diffraction[40] and He scattering[9,42] experiments suggest that the preferential H adsorption site is the threefold coordinated site in the troughs on the Pd(110) surface. In this site, the separation between the hydrogen atom and the two nearest neighbors in the topmost Pd layer, as well as the closest Pd atom in the second layer, is 2 Å. The mutually repulsive interaction between nearest-neighbor hydrogen atoms stabilizes a zigzag adsorption pattern in the troughs on the surface.[9] Results based on the MBA Hamiltonian indicate that this adsorption geometry is slightly energetically disfavored when compared to the preferential long-bridge site. While the MBA Hamiltonian clearly cannot resolve such minute energy differences, we find that the predicted H-Pd interaction potentials are in remarkably good agreement with *ab initio* calculations and experimental data in view of the simplicity of the approach.

IV. PHONON STRUCTURE IN THE BULK AND AT THE SURFACE OF Pd-H SYSTEMS

In this section, we present our phonon calculation results for bulk Pd and PdH, as well as the clean and H-covered (001) and (110) surfaces of Pd. As outlined in Sec. II, the phonon dispersion relations can be determined directly by diagonalizing the dynamical matrix $D_{\alpha\beta,\kappa\nu}(\mathbf{k})$, which is basically a Fourier-transformed force-constant matrix. According to Eq. (11), the force-constant matrix can be determined numerically by calculating total energy differences with respect to the atomic displacements. This can be done efficiently using the MBA Hamiltonian which, as shown above, gives reliable potential energies near the equilibrium structure. It is worthwhile to note that the force-constant matrix accounts for effective second- and third-neighbor interactions. This is a consequence of the many-body nature of the MBA Hamiltonian which correctly describes the indirect interaction between two atoms and its mediation through a third atom neighboring the two sites.

In Fig. 5(a), we compare our phonon calculations for bulk fcc Pd to measured phonon spectra along the high symmetry lines. The experimental data[43] have been obtained using inelastic neutron scattering. As shown in this figure, our calculation is in quite good agreement with the experiment throughout the Brillouin zone. Since

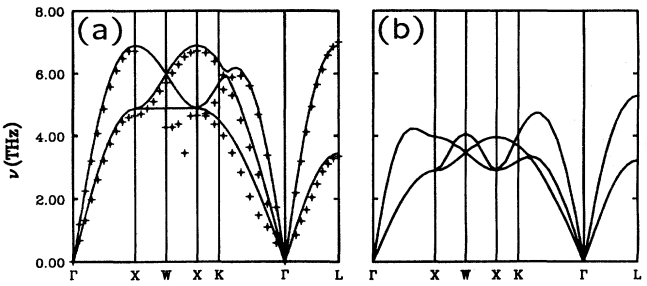

FIG. 5. Phonon dispersion relations for (a) bulk Pd and (b) PdH. Frequencies calculated using the MBA Hamiltonian are given by the solid lines. The experimental data points of Ref. 43 for bulk Pd are given by (+).

our Hamiltonian is based on LDA calculations for static properties of Pd, and does not contain any adjustable parameters, the good agreement indicates that the MBA Hamiltonian also correctly describes the dynamical properties of this system.

The results of our similar calculation for bulk PdH are shown in Fig. 5(b). The net effect of hydrogen on the phonon spectrum is a softening on the acoustic branches. This is partly caused by a 6% increase of the lattice constant upon hydrogen uptake, shown in Fig. 1, from 3.89 Å in Pd to 4.12 Å in PdH. Based on the analysis of our results, we find that the presence of hydrogen has a strong effect on the force-constant matrix Φ. The force constants describing the restoring forces acting on a Pd atom displaced along a high-symmetry direction are reduced from $c = 10.6$ eV/Å^2 in bulk Pd to only 6.8 eV/Å^2 in PdH. The effect of the presence of hydrogen on the bulk modulus is comparably small. We obtain $B = 2.03 \times 10^{12}$ dyn/cm^2 in bulk Pd which compares well with the experimental value[44] $B = 1.81 \times 10^{12}$ dyn/cm^2 and the LDA value of 2.15×10^{12} dyn/cm^2. The corresponding value in PdH is only 3% smaller, $B = 1.98 \times 10^{12}$ dyn/cm^2, which is in fair agreement with the LDA result 1.95×10^{12} dyn/cm^2 of Ref. 5.

Since our main interest is the effect of hydrogen on the Pd modes, we do not include the hydrogen-derived optical modes in the figure. These modes have a very high frequency and are well separated from the acoustic Pd-derived modes due to the mass disparity of these atoms. While the hydrogen atoms can be basically thought of as Einstein oscillators, the weak coupling between hydrogen atoms broadens the optical states to a ≈ 3 THz broadband. Since the H-H nearest-neighbor distance in PdH $r_{0,\text{H-H}} = 2.06$ Å is much larger than the H-H interaction range (≈ 1 Å), we have neglected the direct H-H interaction in our calculation, but have accounted for the dominant indirect interaction mediated by Pd atoms. A closer analysis of the optical bands reveals that two out of the three bands show no dispersion and represent Einstein modes of hydrogen atoms with no direct coupling. The above-mentioned dispersion of the third branch reflects the degree of Pd-mediated indirect interaction between H atoms, which is almost equally strong for the first and second neighbors. These effects in the optical band can also be seen in the measured phonon dispersion relations of the related systems $PdD_{0.63}$ (Ref. 45) and $PdT_{0.7}$.[46]

The calculated phonon spectra for the Pd(100) and Pd(110) surfaces are shown in Figs. 6 and 7, respectively. These surfaces are represented by relaxed 25-layer Pd slabs. Phonon spectra of the clean (001) and (110) Pd surfaces, shown in (a), are compared to results for hydrogen-covered surfaces, shown in (b). In order to distinguish surface from bulk states, we are showing phonon bands of bulk Pd in Figs. 6(c) and 7(c). For the sake of simple comparison, the bulk bands are projected onto the same two-dimensional Brillouin zones in (c) as used in (a) and (b).[47] For both surfaces, our calculations indicate the presence of surface modes which appear either in the bulk band gaps or are split off from the bulk band edges.

Based on the comparison of phonon spectra for Pd(001) in Figs. 6(a) and 6(c), the presence of the surface introduces a soft Rayleigh mode[48] S_1, which is substantially softer than any bulk mode in the Brillouin zone. At the $\bar{M}$ point, this mode corresponds to vibrations of surface atoms perpendicular to the surface. The origin of the mode softening is a decreased interlayer interaction at the surface, which is only partly compensated by the surface contraction. The analysis of our results indicates that the zone-edge frequency of the S_1 mode increases from 3.72 THz for the unrelaxed surface to 4.11 THz for the relaxed surface. A second surface mode S_4, which is barely split from the bulk band at $\bar{M}$, is a transversal mode corresponding to in-plane vibrations. In addition to these soft modes, the surface introduces a phonon mode S_6 with $\nu \approx 6$ THz in the gap of the bulk spectrum near $\bar{X}$. This mode corresponds to in-plane vibrations of topmost layer atoms, coupled to out-of-plane vibrations of second layer atoms.

The phonon spectrum of a hydrogen-covered Pd(001) surface is shown in Fig. 6(b). We have assumed a monolayer coverage corresponding to occupying all hollow sites by H atoms. The Pd surface has been again represented by a 25-layer slab. Similar to the bulk Pd-H system, we are mainly interested in the effect of hydrogen on the Pd surface modes, and do not show the H-derived high-frequency optical modes which are well separated from the Pd modes. The most striking change in comparison to the H-free surface shown in (a) is a massive softening of the Rayleigh mode. At $\bar{M}$, the frequency of the S_1 mode decreases from 4.11 to 2.77 THz due to hydrogen adsorption. On the other hand, hydrogen does harden other modes, such as the bulk band-gap mode at $\nu \approx 6$ THz, which has been discussed above. A detailed analysis of the eigenstates shows that surface phonon modes with a vibration amplitude perpendicular to the surface experience a large amount of softening. Other surface modes with amplitudes restricted to the surface layer, such as the S_6 mode, experience a hardening due to the restricted movement in presence of hydrogen atoms. Our eigenvector analysis also indicates that hydrogen adsorption also increases the confinement of surface modes to the few

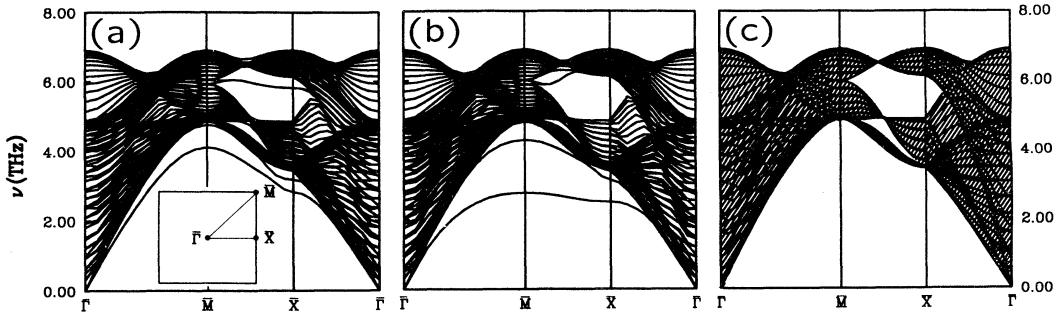

FIG. 6. (a) Calculated phonon dispersion relations for a clean 25-layer Pd slab with a (001) surface. (b) Corresponding results for a H-covered Pd slab (monolayer coverage, hollow site). (c) Bulk phonon dispersion relations of Fig. 5(a), projected onto the two-dimensional surface Brillouin zone used in (a) and (b).

topmost layers and shortens the penetration depth into the bulk.

In Fig. 7, we compare the phonon spectra of clean and hydrogen-covered Pd(110) surfaces to bulk phonon spectra. The Pd surface has been again represented by a 25-layer slab. A comparison of our calculated phonon spectra for clean Pd(110) to inelastic He scattering data of Ref. 15 is shown in Fig. 7(a). The softest surface mode is the Rayleigh mode S_1. Our calculation reproduces the general features of this mode quite well, but our frequencies are $\approx$ 10% higher than the observed data. While we are aware that our parametrized Hamiltonian may not describe the detailed changes of metal bonding at surfaces to a very high accuracy, we cannot exclude the possibility of a slight hydrogen contamination of the Pd sample used in Ref. 15, which is very hard to detect and would also soften the surface Rayleigh mode.

Since Pd(110) shows the largest surface contraction, the softest surface phonon modes are quite close to the lowest lying bulk bands throughout the surface Brillouin zone. The strongest softening can be observed at the $\bar{Y}$ point, where we obtain three surface modes[49] S_1, S_2, and E well below the bulk band. Our analysis of the eigenstates indicates that these modes correspond to in-plane (along the surface x and y directions) and out-of-plane (along the z direction) vibrations of the topmost layer. The lowest mode is an in-plane mode with an amplitude along the y direction. Similar to the (001) surface, the surface contraction generally hardens the surface phonon modes. Our calculation shows that at the $\bar{Y}$ point, because of the relaxation, the lowest surface modes with topmost layer amplitudes along the x, y, and z directions are shifted from 2.36, 2.29, and 2.77 to 2.71, 2.23, and 2.94 THz, respectively.

From the comparison of Figs. 7(a) and 7(c), we see that the presence of the (110) surface introduces several other vibration modes beyond the Rayleigh mode. The bulk phonon spectrum, shown in Fig. 7(c), contains gaps near $\bar{X}$, at $\nu \approx 5.5$ THz, and near $\bar{Y}$, at $\nu \approx 4.5$ THz. On Pd(110), three surface states appear in both gaps. The 5.4-THz gap mode at $\bar{X}$ corresponds to topmost layer atoms vibrating along the surface x direction, and the

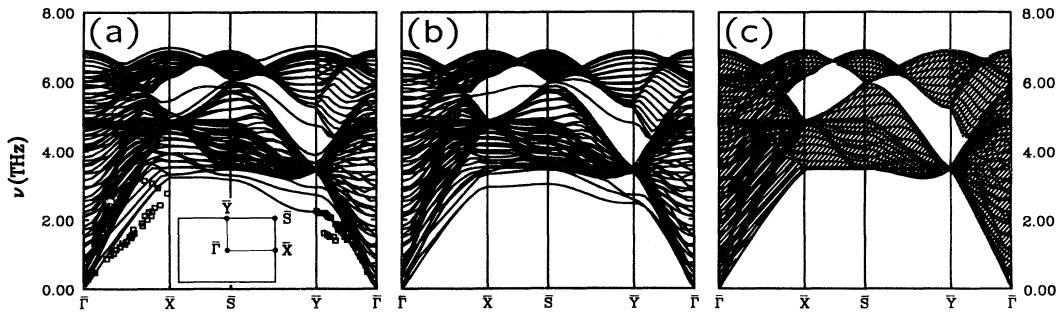

FIG. 7. (a) Calculated phonon dispersion relations for a clean 25-layer Pd slab with a (110) surface. The experimental data of Ref. 15 are given by •. (b) Corresponding results for a H-covered Pd slab (monolayer coverage, long-bridge site). (c) Bulk phonon dispersion relations of Fig. 5(a), projected onto the two-dimensional surface Brillouin zone used in (a) and (b).

4.7-THz gap mode at $\bar{Y}$ corresponds to an analogous vibration along the surface y direction. The surface also introduces high-frequency states slightly above the top of the bulk bands, well visible at the $\bar{X}$ and $\bar{Y}$ points. These modes have considerable amplitudes deep into the bulk, and correspond to alternating in-plane and out-of-plane vibrations on the individual layers.

Calculated surface phonon dispersion relations for the H-covered Pd(110) surface are shown in Fig. 7(b). In analogy to the Pd(001) surface calculation, we have assumed a monolayer coverage corresponding to the occupation of all long-bridge sites (the equilibrium adsorption site) by H. As for bulk PdH and H/Pd(001), we do not show the H-derived high-frequency optical modes for H/Pd(110) in (c). The general trends discussed above for the effect of hydrogen on the surface modes of the Pd(001) surface hold also for the (110) surface. Specifically, we observe a softening of surface modes involving an out-of-plane motion of topmost layer atoms, and a hardening of modes involving an in-plane vibration of surface atoms along the x direction at $\bar{X}$ and the y direction at $\bar{Y}$. Other vibration modes experience very little change.

Hydrogen-induced bonding changes at the Pd(110) surface can be understood by investigating the three lowest phonon modes S_1, S_2, and E at the $\bar{Y}$ point. The S_1 mode, which involves in-plane vibrations of the topmost layer along the surface y direction and out-of-plane vibrations of the second layer, has been pushed up in frequency from 2.23 THz for the clean surface to 2.71 THz for the H-covered surface. The main reason for this hardening is a restricted freedom of motion of topmost layer Pd atoms due to hydrogen atoms adsorbed in the long-bridge site. The S_2 mode, corresponding to a vibration of topmost layer Pd atoms along the close-packed surface x direction, has been softened by the presence of hydrogen from 2.71 THz for the clean surface to 2.46 THz for the H-covered surface. Finally, the E mode, corresponding to out-of-plane vibrations of the topmost layer, experiences the strongest softening from 2.94 THz for the clean surface to 2.56 THz for the H-covered surface.

As compared to the (001) surface, phonon modes at the Pd(110) surface are less affected by hydrogen adsorption. This is especially true for the softening of the Rayleigh mode. This last conclusion may not hold in case of an adsorption in the quasithreefold site discussed in Sec. III. In that case, we would expect an increasing Rayleigh mode softening with increasing hydrogen coverage, which has been observed at the $\bar{Y}$ point on the related Ni(110) surface in high-resolution EELS experiments.[50]

From our calculation, we see that hydrogen adsorption has a profound effect on both the equilibrium structure and dynamical properties of Pd surfaces. These two effects are closely related. The presence of hydrogen adsorbates reverses the topmost layer contraction, and the large anharmonicity of the interlayer interactions causes the effective interlayer force constant to decrease with increasing interlayer distance. This results in a softening of the Rayleigh surface phonon mode with an out-of-plane amplitude in the topmost layer. Since the hydrogen-induced expansion is larger on the more densely packed (001) surface than on the (110) surface, the Rayleigh mode softening is also stronger on the Pd(001) surface.

At both Pd(001) and Pd(110) surfaces, the equilibrium adsorption height of hydrogen is close to zero, i.e., hydrogen atoms are buried inside the topmost Pd layer, where they affect the effective Pd-Pd force constants most. There is very little surface stress associated with this adsorption site, due to the small size of the H atoms. Surface phonon modes with in-plane vibration amplitudes are nearly independent of surface relaxations, but are affected by the presence of hydrogen. This latter effect results from the hydrogen-induced change of Pd-Pd force constants, and also the restricted freedom of motion due to the extra adsorbed atoms which hardens some of these modes.

V. CONCLUSIONS

We have developed a many-body alloy Hamiltonian which describes efficiently total energy changes in alloys such as the Pd-H system. All parameters have been obtained from *ab initio* density-functional calculations, with no adjustable parameters for surface properties. We tested this Hamiltonian first and calculated the equilibrium structure and binding energy of bulk Pd and PdH, as well as H-free and H-covered Pd(001) and Pd(110) surfaces. We found our results to be in good agreement with experimental results where available.

Next, we studied the effect of hydrogen on the vibration spectra of bulk Pd and the Pd(001) and Pd(110) surfaces, by constructing the dynamical matrix based on the MBA Hamiltonian. We find that in the bulk systems, hydrogen softens the Pd vibration modes, as seen in the comparison of bulk Pd and PdH phonon spectra. The results for the clean and H-covered (001) and (110) surfaces of Pd are not as clearcut. We find the most pronounced effect of hydrogen coverage to be the softening of the surface Rayleigh mode with out-of-plane vibration amplitudes on the topmost layer. Other surface modes, such as in-plane vibrations of the topmost layer, are affected to a lesser degree or occur at higher vibration frequencies in the presence of hydrogen.

ACKNOWLEDGMENTS

We thank Z. Sun for useful discussions and helpful comments. This work has been supported by the Office of Naval Research under Contract No. N00014-90-J-1396. CONVEX computer time has been provided by a grant from the Michigan State University.

*Permanent address: Biosym Technologies, Inc., 10065 Barnes Canyon Road, San Diego, CA 92121-2777.

[1] *Hydrogen in Metals I and II*, edited by G. Alefeld and J. Völkl, Topics in Applied Physics Vols. 28 and 29 (Springer-Verlag, Berlin, 1978).

[2] H. K. Birnbaum, M. Grossbeck, and S. Gahr, in *Hydrogen in Metals*, edited by M. Bernstein and A. Thompson, (ASM, Metals Park, OH, 1973), p. 303; H.K. Birnbaum,

in *Environmentally Sensitive Fracture of Engineering Materials*, edited by Z. A. Foroulis (TMS, New York, 1979), p. 326.
[3] D. Tománek, S.G. Louie, and C.T. Chan, Phys. Rev. Lett. **57**, 2594 (1986).
[4] Z. Sun and D. Tománek, Phys. Rev. Lett. **63**, 59 (1989).
[5] D. Tománek, Z. Sun, and S.G. Louie, Phys. Rev. B **43**, 4699 (1991).
[6] M.G. Cattania, K. Christmann, V. Penka, and G. Ertl, Gazz. Chim. Ital. **113**, 433 (1983).
[7] J.-W. He, D.A. Harrington, K. Griffiths, and P.R. Norton, Surf. Sci. **198**, 413 (1988).
[8] R.J. Behm, K. Christmann, and G. Ertl, Surf. Sci. **99**, 320 (1980).
[9] K.H. Rieder, M. Baumberger, and W. Stocker, Phys. Rev. Lett. **51**, 1799 (1983).
[10] K.H. Rieder and W. Stocker, Surf. Sci. **148**, 139 (1984).
[11] B. Tardy and J.C. Bertolini, C. R. Acad. Sci. Ser. 2 **302**, 813 (1986).
[12] C. Nyberg and C.G. Tengstål, Phys. Rev. Lett. **50**, 1680 (1983).
[13] F. Besenbacher, I. Stensgaard, and K. Mortensen, Surf. Sci. **191**, 288 (1987).
[14] J.P. Toennies, J. Vac. Sci. Technol. A **5**, 440 (1987); **2**, 1055 (1984).
[15] A.M. Lahee, J.P. Toennies, and Ch. Wöll, Surf. Sci. **191**, 529 (1987).
[16] R.B. Doak, U. Harten, and J.P. Toennies, Phys. Rev. Lett. **51**, 578 (1983).
[17] U. Harten, J.P. Toennies, Ch. Wöll, and G. Zhang, Phys. Rev. Lett. **55**, 2308 (1985).
[18] H. Ibach, J. Vac. Sci. Technol. A **5**, 419 (1987).
[19] S. Lehwald, J.M. Szeftel, H. Ibach, T.S. Rahman, and D.L. Mills, Phys. Rev. Lett. **50**, 518 (1983); M. Rocca, S. Lehwald, H. Ibach, and T.R. Rahman, Surf. Sci. **138**, L123 (1984).
[20] M. Wuttig, R. Franchy, and H. Ibach, Solid State Commun. **57**, 445 (1986).
[21] J. Yoshinobu, M. Onchi, and M. Nishijima, Phys. Rev. B **38**, 1520 (1988).
[22] W. Kohn and L.J. Sham, Phys. Rev. **140**, A1133 (1965).
[23] K.-M. Ho and K.P. Bohnen, Phys. Rev. Lett. **56**, 934 (1986).
[24] R.A. Johnson, Phys. Rev. B **6**, 2094 (1972).
[25] V. Bortolani, G. Santoro, U. Harten, and J.P. Tonnies, Surf. Sci. **148**, 82 (1984).
[26] V. Bortolani, A. Franchini, F. Nizzoli, and G. Santoro, Surf. Sci. **152/153**, 811 (1985).
[27] B.M. Hall, D.L. Mills, M.H. Mohamed, and L.L. Kesmodel, Phys. Rev. B **38**, 5856 (1988).
[28] M.S. Daw and M.I. Baskes, Phys. Rev. B **29**, 6443 (1984); S.M. Foiles, *ibid.* **32**, 3409 (1985); Surf. Sci. **191**, L779 (1987); M.S. Daw, Phys. Rev. B **39**, 7441 (1989); S.M. Foiles and J.B. Adams, *ibid.* **40**, 5909 (1989).
[29] J.S. Nelson, E.C. Sowa, and M.S. Daw, Phys. Rev. Lett. **61**, 1977 (1988).
[30] J.S. Nelson, M.S. Daw, and E.C. Sowa, Phys. Rev. B **40**, 1465 (1989).
[31] N. Luo, W. Xu, and S.C. Shen, Solid State Commun. **67**, 837 (1988).
[32] D. Tománek, S. Mukherjee, and K.H. Bennemann, Phys. Rev. B **28**, 665 (1983); **29**, 1076(E) (1984).
[33] D. Tománek, Phys. Lett. **113A**, 445 (1986); D. Tománek and K.H. Bennemann, Surf. Sci. **163**, 503 (1985).
[34] D. Tománek, A.A. Aligia, and C.A. Balseiro, Phys. Rev. B **32**, 5051 (1985).
[35] D. Spanjaard and M.C. Desjonquères, Phys. Rev. B **30**, 4822 (1984).
[36] D.W. Brenner, Phys. Rev. Lett. **63**, 1022 (1989).
[37] A.A. Maradudin, E.W. Montroll, and G.H. Weiss, *Theory of Lattice Dynamics In The Harmonic Approximation* (Academic, New York, 1963).
[38] H.L. Davis and J.R. Noonan, Surf. Sci. **126**, 245 (1983).
[39] C.J.Barnes, M.Q. Ding, M. Lindroos, R.D. Diehl, and D.A. King, Surf. Sci. **162**, 59 (1985).
[40] M. Skottke, R.J. Behm, G. Ertl, V. Penka, and W. Moritz, J. Chem. Phys. **87**, 6191 (1987).
[41] K.P. Bohnen, Th. Rodach, and K.M. Ho, in *The Structure of Surfaces III*, edited by M.A. Van Hove, K. Takanayagi, and X. Xie (Springer-Verlag, Heidelberg, 1990), and references cited therein.
[42] R. Bastasz, T.E. Felter, and W.P. Ellis, Phys. Rev. Lett. **63**, 558 (1989).
[43] A.P. Miller and B.N. Brockhouse, Can. J. Phys. **49**, 704 (1971).
[44] Ch. Kittel, *Introduction to Solid State Physics*, 6th ed. (Wiley, New York, 1986).
[45] J.M. Rowe, J.J. Rush, H.G. Smith, M. Mostoller, and H.E. Flotow, Phys. Rev. Lett. **33**, 1297 (1974).
[46] J.M. Rowe, J.J. Rush, J.E. Schirber, and J.M. Mintz, Phys. Rev. Lett. **57**, 2955 (1986).
[47] This procedure yields continuous bulk bands at each **k** point in the Brillouin zone. The apparent discreteness in Figs. 6(c) and 7(c) results from a finite **k**-point sampling in a direction perpendicular to the Brillouin zone.
[48] For the labeling of the phonon branches, see, e.g., Ref. 29.
[49] For the labeling of the phonon branches, see, e.g., Ref. 15.
[50] S. Lehwald, B. Voigtländer, and H. Ibach, Phys. Rev. B **36**, 2446 (1987).